

Fourier transform infrared spectrum: Vibrational assignments using density functional theory and natural bond orbital analysis of the bis(guanidoacetate)nickel(II) complex

Joanna M. Ramos^a, Maurício T. de M. Cruz^a, Anilton C. Costa Jr.^{a,b}, Otávio Versiane^b, Claudio A. Téllez Soto^{a,*}

^a Departamento de Química Inorgânica, Instituto de Química, Universidade Federal Fluminense (UFF), Morro do Valonguinho s/n, Niterói-Centro CEP 24210-150, RJ, Brazil

^b Centro Federal de Educação Tecnológica de Química de Nilópolis (CEFETEQ) Unidade de Rio de Janeiro, Rio de Janeiro, RJ, Brazil

*Corresponding author, e-mail: tellez@vm.uff.br

Received 11 Jun 2010

Accepted 14 Jul 2011

ABSTRACT: Theoretical and experimental band assignments for the Fourier transform infrared spectrum of the $[\text{Ni}(\text{GAA})_2] \cdot 2\text{H}_2\text{O}$ (bis(guanidoacetate)nickel(II) complex) *trans* isomer has been made based on the DFT: B3LYP/6-311G(d,p) procedure, second derivative spectrum, and band deconvolution analysis. Bond orbital analysis was used to determine the effect of electronic delocalization involving Ni–O and Ni–N bonds and their neighbour groups. Also, natural bond orbital analysis was extended to Ni–O and Ni–N interactions, indicating in both cases that the $sp^{2.01}d^{1.01}$ Ni(II) hybridization is adequate for the planar structure around the Ni(II) cation. The calculated infrared spectrum, based on the proposed geometrical structure of the *trans* bis(guanidoacetate)nickel(II) complex without crystallization water, shows an excellent agreement with the experimental spectrum, and matches better than the calculated spectra for the $[\text{Ni}(\text{GAA})_2]$ *cis* isomer. The calculated energy for the $[\text{Ni}(\text{GAA})_2]$ *trans* isomer complex is 21.75 kcal/mol more stable than that of the *cis* isomer.

KEYWORDS: vibrational spectra, nickel(II) guanidoacetate complex, quantum mechanical calculations

INTRODUCTION

The importance of divalent nickel in biological and bioinorganic compounds was summarized in previous papers^{1–3}. In Ref. 4, fourteen articles by leading researchers are devoted exclusively to biological use of nickel. The content ranges from the chemistry and physics of nickel complexes in general to the roles of this metal in cellular catalytic phenomena. A recent article on synthesis, spectroscopic, and antimicrobial studies of divalent nickel⁵, and another on nickel ion reduction with applications to the analysis of nutritional supplements⁶ are examples reflecting the biological importance of divalent nickel.

Continuing our vibrational spectroscopic studies on metal-amino acid complexes^{7–9}, we have made a full vibrational assignment based on the Fourier transform infrared spectrum, second derivative spectrum, band deconvolution analysis, and density functional theory (DFT)/B3LYP:6-311G(d,p) calculations¹⁰. We considered the structural geometry of the *trans*-

bis(guanidoacetate)Ni(II) complex, and the natural bond orbital analysis to study Ni(II) hybridization conducting to the planar geometry of the framework.

EXPERIMENTAL

Synthesis of the bis(guanidoacetate)nickel(II) complex $[\text{Ni}(\text{GAA})_2] \cdot 2\text{H}_2\text{O}$

Synthesis was done according to the procedure described by Versiane¹¹. Guanidoacetic acid (H_3GAA) dissolves poorly in water. Hot dissolution produces immediate crystallization after freezing. In alkaline solutions, decomposition occurs with loss of the guanidinic group GAA^{3+} . Fig. 1 shows a diagram of species distribution as a function of pH. The synthesis conditions for the low solubility of H_3GAA were determined based on the crossing of $\text{Ni}(\text{OH})_2$ solubility curve with the curve on species distribution diagram for H_3GAA . Temperature was maintained below 47 °C to avoid H_3GAA crystallization. The synthesis of the $[\text{Ni}(\text{GAA})_2] \cdot 2\text{H}_2\text{O}$ complex is limited to the

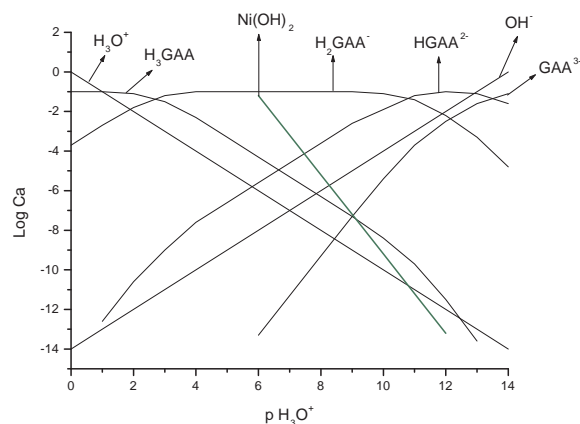


Fig. 1 Overlap between the species distribution diagram of H_3GAA and the $\text{Ni}(\text{OH})_2$ formation diagram.

proportion of 2 mmols of H_3GAA (0.2342 g) in 50 ml of water. Any alteration whatsoever such as higher concentration or higher temperature leads to a contamination of the final product with H_3GAA . For this reason, the $[\text{Ni}(\text{GAA})_2] \cdot 2\text{H}_2\text{O}$ complex was prepared by dissolving 2 mmols of H_3GAA in 50 ml of deionized water under strong stirring for 2 h at 28 °C (room temperature). After the complete dissolution of the ligand, the solution was frozen at 4 °C for 1 h, and then left at room temperature for 3 days. Any precipitate formed was dissolved by water addition until the system reached equilibrium and did not crystallize any H_3GAA under minor temperature variations. At this stage of the synthesis, 1 mmol of $\text{Ni}(\text{NO}_3)_2$ was added to the ligand solution under stirring for 4 h. The temperature was adjusted to 45 °C and the system was left under stirring for 19 h, after which the temperature was lowered to room temperature. After two days, the solution was warmed again to 45 °C and the pH was adjusted to 3.4 by adding KOH 3 M. After the open solution was left at room temperature for 7 days, a green and clear solution of 1/3 of the initial volume was obtained. After addition of 5 ml of ethanol the solution was kept in a closed vessel for 3 days. Then, the solution was evaporated at room temperature to give a green amorphous solid. The yield was 48%.

Elemental analysis

All the analysis was carried out in the same conditions and with the same CHN column. After the stabilization stage, we observed that any change in the column, or the analysis of different samples, produced small variations of the order of 2%. After three weeks, the samples were analysed again. The final results reflect the arithmetic mean of the results with fluctuations

lower than 2%. For the $[\text{Ni}(\text{GAA})_2] \cdot 2\text{H}_2\text{O}$ complex we found the following values (the theoretical composition is given in parentheses): C: 22.00% (22.04%), H: 4.97% (4.90%), N: 25.61% (25.70%), O: 29.44% (29.39%). Ni was analysed by atomic absorption spectrometry yielding the experimental value of 17.95% (17.97%).

Thermo-gravimetric analysis

The thermo-gravimetric analysis was performed in an inert N_2 atmosphere. The results of the thermo-gravimetric analysis in the temperature range of 100–215 °C showed a mass loss of 36.4%, which corresponds to an experimental value of 122 g (119 g calculated). This loss of mass corresponds to the fragments: 2 (CN_2H_3) and 2 H_2O . At temperatures of 215–900 °C, the mass loss was of 27.6%, which corresponds to the experimental value of 84 g (90 g calculated). This mass loss is attributable to 2 (CO) and 2 (CH_2) . At temperatures above 900 °C the mass loss was 36 g, attributable to NiO_2 and N_2 .

FT-IR spectrum

The Fourier transform infrared (FT-IR) spectra of solid nickel(II) complex were recorded on a Perkin Elmer 2000 FT-IR spectrometer. Data were collected at a resolution of 4 cm^{-1} . The scanning speed was held at 0.2 $\text{cm}^{-1}\text{s}^{-1}$ and 120 scans were performed. The solid sample was measured as a KBr pellet in the 4000–370 cm^{-1} spectral range, and in the 700–30 cm^{-1} region as polyethylene pellet. Observed infrared spectra in both regions are given in Fig. 2.

Optimization of the geometrical parameters

The geometry optimization of the bis(guanidoacetate) nickel(II) complex, $[\text{Ni}(\text{GAA})_2] \cdot 2\text{H}_2\text{O}$, was done using the DFT procedure with the B3LYP/6-311G(d,p) level¹⁰. The calculated energy for the complex in the *trans* form is 21.75 kcal/mol more stable than the *cis* isomer, so hereafter we are dealing only with the *trans*- $[\text{Ni}(\text{GAA})_2] \cdot 2\text{H}_2\text{O}$ complex. The calculated bond lengths for both Ni–N bonds are 1.965 Å, a value that can be compared with the experimental Ni–N bond length of 2.047 Å found in the $[\text{Ni}(\text{L}-\text{aspO})(\text{H}_2\text{O})_2] \cdot \text{H}_2\text{O}$ complex¹², and with the calculated values of the aspartate hydroxo-aqua Ni(II) complex, $[\text{Ni}(\text{Asp})(\text{OH})(\text{H}_2\text{O})]$, using the DFT procedure with B3LYP/6-31G(d) and B3LYP-6-311G(d,p) levels, which are 1.824 and 1.892 Å, respectively¹. For Ni–O bond lengths the calculated value is 1.840 Å. The Ni–O calculated bond lengths for $[\text{Ni}(\text{Gly})(\text{GAA})]$ complex are 1.852 and 1.852 Å², values that agree well with the

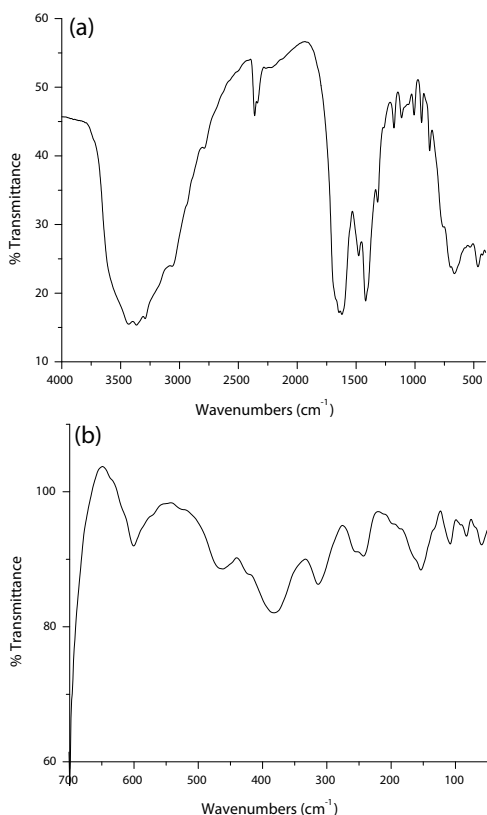


Fig. 2 FT-IR spectra of $[\text{Ni}(\text{GAA})_2] \cdot 2 \text{H}_2\text{O}$ in the (a) 4000–400 cm^{-1} and (b) 700–30 cm^{-1} regions.

DFT/B3LYP/6-31G(d) calculated Ni–O bond lengths for the $[\text{Ni}(\text{Ser})_2]$ complex, whose values are 1.844 and 1.853 \AA ³. For the $[\text{Ni}(\text{Asp})(\text{OH})(\text{H}_2\text{O})]$ complex the DFT values for Ni–O bonds are 1.751, 1.818, and 1.854, 1.906 \AA , with the same basis set indicated above. Experimental values for Ni–O bonds for $[\text{Ni}(\text{L}-\text{aspO})(\text{H}_2\text{O})_2] \cdot \text{H}_2\text{O}$ are 2.063 and 2.064 \AA . Concerning the calculated bond angles, the mean value of the ratio between NNiN (179.20°) and ONiO (177.38°) divided by two gives a factor $\beta = 89.15^\circ$ ¹³, indicating a slight deviation from the planar framework structure. Selected bond lengths and bond angles are given in Table 1. Full $[\text{Ni}(\text{GAA})_2]$ complex structure is given in Fig. 3.

Natural bond orbital analysis (NBO)

NBO analysis¹⁴ at the B3LYP/6-311G(d,p) level was carried out to rationalize the factors contributing to the total conformational energy. The NBO analysis for the isolated complex shows that the nickel(II) ion interacts more strongly with oxygen than with nitrogen. The calculated second-order perturbation

Table 1 DFT/B3LYP/6-311G(d,p) calculated framework geometrical parameters for the bis(guanidoacetate)nickel(II) complex.

| Bond lengths | (\AA) | Bond angles | ($^\circ$) |
|--------------|------------------|-------------------|--------------|
| Ni(1)–N(2) | 1.966 | N(2)–Ni(1)–N(17) | 179.20 |
| Ni(1)–O(15) | 1.840 | Ni(1)–N(2)–C(10) | 108.50 |
| Ni(1)–O(16) | 1.840 | O(15)–Ni(1)–O(16) | 177.38 |
| Ni(1)–N(17) | 1.966 | Ni(1)–O(15)–C(13) | 116.81 |
| N(2)–C(10) | 1.494 | O(16)–Ni(1)–N(17) | 86.82 |
| C(10)–C(13) | 1.485 | Ni(1)–N(17)–C(25) | 108.50 |
| C(13)–O(15) | 1.363 | N(2)–C(10)–C(13) | 112.83 |
| O(16)–C(28) | 1.363 | C(10)–C(13)–O(15) | 113.58 |
| N(17)–C(25) | 1.494 | O(16)–C(28)–C(25) | 113.58 |
| C(25)–C(28) | 1.485 | N(17)–C(25)–C(28) | 112.83 |
| O(15)–H(21)* | 1.787 | | |
| O(16)–H(9)* | 1.821 | | |

* Hydrogen bonding

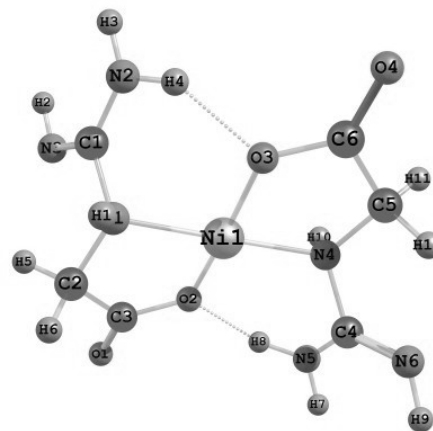


Fig. 3 DFT/B3LYP/6-311G(d,p) calculated structure of the $[\text{Ni}(\text{GAA})_2]$ complex with atom numbering. (Crystallization water was omitted).

energy for the Ni(1)–O(16) interaction is 8.4 kcal/mol greater than for Ni(1)–N(17) (41.3 versus 32.9 kcal/mol, respectively). The Ni–O bond is formed by interaction between a $sp^{2.04}d^{1.04}$ (24.47% *s*, 50.01% *p*, and 25.53% *d*) orbital centred on the nickel ion and a $sp^{1.8}$ (35.76% *s* and 64.24% *p*) orbital on the oxygen atom (Fig. 4b). The Ni–N bonding is formed by the interaction between a $sp^{2.01}d^{1.01}$ (24.91% *s*, 50.02% *p*, and 25.06% *d*) orbital centred on the nickel and a $sp^{4.33}$ (18.77% *s* and 81.23% *p*) orbital on the nitrogen atom (Fig. 4c). The polarization coefficient for the formation of the bonding is 8.84% on the nickel ion and 91.16% on the oxygen atom of the Ni–O bond, and 7.31% on the nickel ion and 92.69%

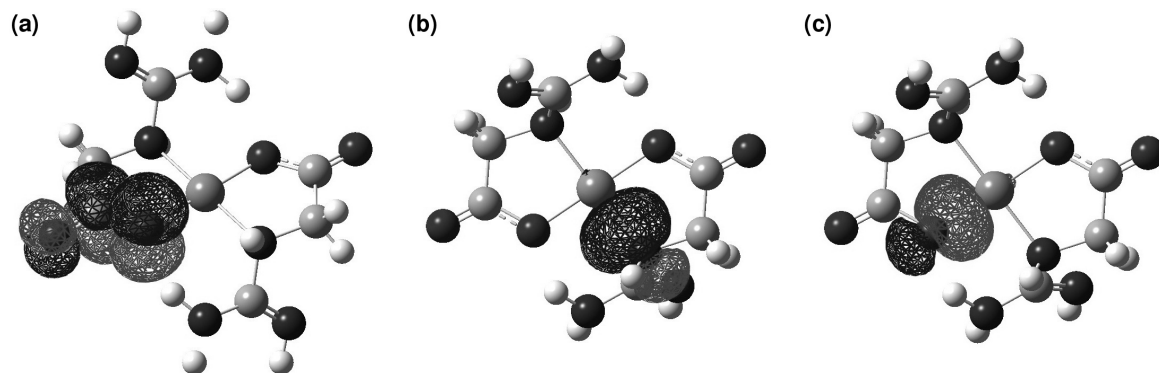


Fig. 4 Natural bond orbital analysis: (a) overlap between a $\pi^* \text{C}=\text{O}$ antibonding orbital and a p_z orbital on the oxygen atom of the Ni–O bond; (b) natural bond orbital between nickel and nitrogen atom; and (c) natural bond orbital between nickel and oxygen atom.

on the nitrogen atom of the Ni–N bond. These results show a high polarization directed to the oxygen and nitrogen atoms in the Ni–O and Ni–N bonding, respectively, indicating a strong ionic character on both bonds. In addition, analysis performed over the electronic effects of the ligands on the nickel complex shows that, after the complex was formed, the energy involved in electronic delocalization between the O (15 or 16) and N (2 or 17) atoms and its C=O and C=N neighbour groups, respectively, diminish if we compare with this delocalization effect in the free ligand. The NBO calculations show that the energy involved in the overlapping between a p_z orbital on the O of the Ni–O bond and the $\pi^* \text{C}=\text{O}$ antibonding orbital (Fig. 4a) is about 30.0 kcal/mol less than that of the isolated ligand (21.86 vs 51.73 kcal/mol, respectively). The same behaviour was found in the overlapping of a p_z orbital on the nitrogen atom of the Ni–N bond with the $\pi^* \text{C}=\text{N}$ antibonding orbital. The energy was 6.0 kcal/mol lower than that of the isolated ligand (6.28 vs 12.65 kcal/mol, respectively). This decrease in the electronic delocalization energy must be a consequence of the increase in the charge density over the oxygen and nitrogen atoms as they bind to the nickel metal. The increase in charge density on O(16) and N(17) (and in its symmetric ones) causes an elongation in the O(16)–C(28) and N(17)–C(28) bonding (complex: O(16)–C(28) = 1.363 Å and N(17)–C(28) = 1.493 Å; ligand free: O(16)–C(28) = 1.298 Å and N(17)–C(28) = 1.411 Å). These elongations reduce the overlap degree accountable to electronic delocalization. Also, in connection with the NBO analysis, the stabilization energies of the LP(1) O(16) with the LP*(1) H(9), and LP(1) O(15) with the LP*(1) H(21), were found to be both of 6.32 kcal/mol.

RESULTS AND DISCUSSION

The $3n - 6 = 81$ normal modes of the $[\text{Ni}(\text{GAA})_2]$ complex can be described by 32 stretching, 58 bending, and 20 torsion internal co-ordinates, including redundant co-ordinates. With the exception of the N–H and C–H stretching of higher vibrational energy, the remaining stretching modes, including the C=O stretching, can be found as coupled modes because there are other internal co-ordinates which describes the normal modes as a whole, such as H–N–H bending. Overlapped bands are expected in the high energy region of the spectrum ($3500\text{--}2700\text{ cm}^{-1}$), and also in the whole mid-IR spectrum. To characterize these bands we used deconvolution analysis, and we have also calculated the second derivative of the band spectrum. A plot between the calculated and the experimental wavenumbers generates a straight line with a correlation coefficient $R = 0.9939$, showing a very good agreement.

N–H and C–H stretching

The $-\text{NH}_2$ and $-\text{NH}$ groups in the molecular structure of $[\text{Ni}(\text{GAA})_2]$ complex provide 8 stretching normal modes. The pairs of infrared bands found at $3603/3526\text{ cm}^{-1}$ and $3444/3367\text{ cm}^{-1}$ by deconvolution analysis can be assigned to the $\nu_{\text{as}}(\text{NH})/\nu_{\text{s}}(\text{NH})$ stretching vibrational modes as this pair of bands follows the Bellamy-Williams wavenumber relation $\nu_{\text{s}}(\text{NH}) = 345.53 + 0.876\nu_{\text{as}}(\text{NH})^{15}$. The other bands found at 3289, 3187, 3087, and 3039 cm^{-1} can be assigned to the $\nu(\text{NH})$ stretching of the imine and R_2NH groups present in the complex structure. In Table 2 the experimental assignments disagree with the wavenumber assignment obtained by the DFT/B3LYP:6-311G(d,p) calculations.

Table 2 DFT:B3LYP/6-311G(d,p) calculated and FT-IR experimental wavenumbers of [Ni(GAA)₂]. (Units: cm⁻¹).

| DFT(calc) | x0.9613 | <i>I</i> _{IR} ^b | IR (%T) | 2d.der. ^c | BDA ^d | Approximate assignment ^a |
|-----------|---------|-------------------------------------|-----------|----------------------|------------------|--|
| | | | | 3646 | | $\nu(\text{OH})$.cryst.water* |
| | | | 3511 | 3616 | 3572 | $\nu(\text{OH})$.cryst.water* |
| 3681 | 3539 | 49.2 | | | | $\nu_{\text{as}}(\text{NH})$ |
| 3664 | 3522 | 43.7 | 3511 (29) | | | $\nu_{\text{as}}(\text{NH})/\nu_{\text{s}}(\text{NH})$ |
| 3484 | 3349 | 9.5 | 3436 (33) | 3440 | 3444 | $\nu(\text{NH})$ imine/ $\nu_{\text{as}}(\text{NH})$ |
| 3482 | 3347 | 8.5 | 3366 (34) | 3367 | 3367 | $\nu(\text{NH})$ imine/ $\nu_{\text{s}}(\text{NH})$ |
| 3465 | 3331 | 17.9 | 3293 (35) | 3287 | 3289 | $\nu(\text{NH})-(\text{R}_2\text{NH})$ |
| 3452 | 3318 | 16.8 | 3201 (28) | 3162 | 3187 | $\nu(\text{NH})-(\text{R}_2\text{NH})$ |
| 3347 | 3217 | 441.6 | | 3103 | 3087 | $\nu_{\text{s}}(\text{NH})$ |
| 3319 | 3191 | 419.0 | 3060 (26) | 3050 | 3039 | $\nu_{\text{s}}(\text{NH})$ |
| 3139 | 3018 | 7.2 | | 2989 | 2987 | $\nu_{\text{as}}(\text{CH})$ |
| 3118 | 2997 | 17.1 | 2939 (18) | 2939 | 2934 | $\nu_{\text{as}}(\text{CH})$ |
| 3070 | 2951 | 17.4 | 2891 (15) | 2883 | 2883 | $\nu_{\text{s}}(\text{CH})$ |
| 3063 | 2944 | 33.4 | | 2850 | | $\nu_{\text{s}}(\text{CH})$ |
| 1739 | 1671 | 222.5 | 1701 (15) | 1702 | 1690 | $\delta(\text{HNH})$ sciss. |
| 1733 | 1666 | 82.9 | | 1676 | 1670 | Q(C=N) |
| 1731 | 1664 | 298.4 | 1649 (24) | 1649 | 1650 | Q(C=N) |
| 1727 | 1660 | 485.2 | 1621 (24) | 1620 | 1621 | $\delta(\text{HNH}) + \text{Q}(\text{C}=\text{O})$ |
| 1685 | 1620 | 170.0 | | 1598 | 1595 | Q(C=O) + $\delta(\text{HNH})$ |
| 1679 | 1614 | 420.0 | 1552 (6) | 1550 | 1542 | Q(C=O) + $\delta(\text{HNH})$ |
| 1513 | 1454 | 14.5 | | 1526 | 1521 | $\delta(\text{HCH})$ sciss. |
| 1480 | 1423 | 30.3 | 1477 (12) | 1477 | 1479 | $\delta(\text{HCH})$ sciss. |
| 1467 | 1410 | 54.0 | 1420 (21) | 1422 | 1423 | $\delta(\text{HCH})$ wagg. |
| 1460 | 1403 | 54.0 | 1399 (19) | 1391 | 1402 | $\delta(\text{NH})$ |
| 1399 | 1345 | 62.6 | | | 1345 | $\delta(\text{HCH}) + \delta(\text{NH})$ |
| 1390 | 1336 | 70. | | | 1336 | $\delta(\text{HCH}) + \delta(\text{NH})$ |
| 1378 | 1325 | 41.2 | 1316 (12) | 1315 | 1316 | $\delta(\text{HCH}) + \delta(\text{NH})$ |
| 1365 | 1312 | 15.5 | | | 1306 | $\delta(\text{HCH}) + \delta(\text{NH})$ |
| 1307 | 1256 | 18.4 | 1262 (4) | 1258 | 1258 | $\delta(\text{HCH})$ twist |
| 1297 | 1247 | 36.6 | | 1234 | 1228 | $\delta(\text{HCH})$ twist |
| 1277 | 1228 | 88.0 | | | 1190 | p(CO) + p(CC) |
| 1264 | 1215 | 484.5 | | | 1177 | p(CO) + p(CC) |
| 1198 | 1152 | 128.6 | 1177 (7) | 1171 | 1156 | $\delta(\text{HNH})$ wagg. |
| 1174 | 1129 | 64.1 | 1115 (8) | 1116 | 1114 | $\delta(\text{HNH})$ wagg. |
| 1153 | 1108 | 45.5 | | | 1088 | $\delta(\text{NH}) + \delta(\text{HCH})$ |
| 1132 | 1088 | 37.1 | 1051 (6) | 1050 | 1066 | $\delta(\text{NH}) + \delta(\text{HCH})$ |
| 1079 | 1037 | 87.7 | | | 1047 | p(CN) + $\delta(\text{NH})$ |
| 1076 | 1034 | 135.1 | 1008 (7) | 1007 | 1008 | p(CN) + $\delta(\text{NH})$ |
| 1029 | 989 | 63.7 | | | | p(CN) + $\delta(\text{NH})$ |
| 1024 | 984 | 61.4 | | | | p(CN) + $\delta(\text{NH})$ |
| 1015 | 976 | 36.8 | | | | $\rho(\text{CH}_2) + \text{p}(\text{CN})$ |
| 1002 | 963 | 3.4 | 943 (7) | 944 | 944 | $\rho(\text{CH}_2) + \rho(\text{NH})$ |
| 927 | 891 | 53.1 | | 910 | 905 | p(CC) + p(CO) |
| 912 | 877 | 15.5 | 876 (8) | 876 | 875 | p(CC) + p |
| 864 | 831 | 115.6 | | 829 | 824 | p(CN) + $\rho(\text{NH})$ |
| 839 | 807 | 10.3 | | | | $\rho(\text{NH})_{\text{as}}$ |
| 830 | 798 | 128.7 | | | | $\rho(\text{NH})_{\text{s}}$ |
| 823 | 791 | 83.2 | | | | $\rho(\text{NH})$ |
| 814 | 782 | 256.6 | 773 (1) | 782 | 766 | $\rho(\text{NH})$ |
| 800 | 769 | 395.8 | 722 (3) | 721 | 720 | $\rho(\text{NH})(-\text{NH}_2)$ |
| 780 | 750 | 8.2 | 706 (14) | 703 | 712 | p(CN) + $\delta(\text{CNC})$ |
| 740 | 711 | 2.1 | | | 700 | $\delta(\text{CONi}) + \delta(\text{CCO})$ |
| 712 | 684 | 15.4 | 672 (18) | 669 | 664 | $\rho(\text{NH}_2)$ |

Table 2 (Cont.)

| DFT(calc) | x0.9613 | I_{IR}^b | IR (%T) | 2d.der. ^c | BDA ^d | Approximate assignment ^a |
|-----------|---------|------------|----------|----------------------|------------------|---|
| 699 | 672 | 2.1 | 648 (17) | 637 | 637 | $\rho(NH_2)$ |
| 667 | 641 | 36.0 | 632 (15) | 622 | 626 | $\delta(CNC)$ |
| 657 | 632 | 7.1 | 600 (6) | 594 | 593 | $\delta(CNC)$ |
| 593 | 570 | 45.7 | 569 (7) | 568 | 569 | $\delta(NC=N)$ |
| 582 | 559 | 2.2 | 551 (4) | 547 | 547 | $\delta(NC=N)$ |
| 535 | 514 | 6.0 | 529 (1) | 527 | 522 | $\rho(C=O)$ |
| 528 | 508 | 4.6 | | | 500 | $\rho(C=O)$ |
| 508 | 488 | 37.5 | 470 (5) | 468 | 480 | $\rho(NH)$ |
| 493 | 474 | 27.6 | | | 469 | $\rho(NH)$ |
| 475 | 457 | 51.0 | | | 452 | $r(NiO)$ 27% + $\beta(NNiO)$ 25% |
| 463 | 445 | 21.7 | 427 (2) | 425 | 425 | $r(NiN)$ 14% + $\beta(NNiO)$ 10% |
| 454 | 436 | 77.0 | | | 409 | $r(NiN)$ 29% + $\beta(NNiO)$ 17% |
| 434 | 417 | 4.0 | | | | $\beta(NNiO)$ 36% |
| 418 | 402 | 4.6 | 382 (8) | | 391 | $\beta(NNiO)$ 18% + $r(NiO)$ 14% |
| 383 | 368 | 44.0 | | 373 | 373 | $\beta(NNiO)$ 26% + $\beta(NiNC)$ 14% |
| 360 | 346 | 5.6 | | | | $r(NiN)$ 26% + $r(NiO)$ 21% |
| 336 | 323 | 6.2 | 313 (9) | | 359 | $\tau(\text{bent } N(2)-C(13) \text{ axis})$ |
| 315 | 303 | 4.5 | | 313 | 317 | $\tau(\text{bent } N(17)-C(25) \text{ axis})$ |
| 278 | 267 | 0.9 | 255 (8) | | 305 | $r(NiO)$ 27% + $\beta(NNiO)$ 18% |
| 249 | 239 | 19.1 | 246 (9) | 259 | 256 | $\beta(NNiO)$ 37% + $\beta(NiNC)$ 12% |
| 238 | 229 | 2.9 | | 240 | 240 | $\beta(NNiO)$ 47% + $\beta(NiNC)$ 13% |
| 209 | 201 | 1.3 | 199 (3) | 200 | 204 | $\beta(NNiO)$ 43% + $\beta(NiNC)$ 14% |
| 136 | 131 | 19.9 | 153 (12) | 154 | 154 | τ + $\beta(NNiO)$ |
| 113 | 109 | 5.0 | 112 (6) | 108 | 108 | $\tau(NiOCC)$ |
| 101 | 97 | 0.6 | 89 (8) | 84 | 82 | $\tau(NiOC=O)$ |
| 82 | 79 | 0.2 | | | 69 | $\tau(NiNCN)$ |
| 59 | 57 | 5.6 | 56 (12) | 56 | 59 | $\tau(O=CCN)$ |
| 52 | 50 | .0 | | | | $\tau(CNC=NH)$ |
| 40 | 38 | 7.0 | 33 (1) | | | $\tau(NCCO)$ |
| 17 | 16 | 0.3 | | | | $\tau(NiNCC)$ |

^a means participation of different internal coordinates in the normal mode composition, according to the geometrical parameter variation that composes it;

^b I_{IR} mean infrared intensities;

^c 2d.der. mean second derivatives;

^d BDA means band deconvolution analysis.

Concerning the C–H stretching we expected only four infrared absorptions which were found at 2987, 2934, and 2883, and at 2850 cm^{-1} by deconvolution analysis, the last one being observed in the second derivative spectrum. The two higher wavenumbers were assigned to the $\nu_{as}(\text{CH})$ stretching and the remainder to the $\nu_s(\text{CH})$ stretching. Fig. 5 shows the band deconvoluted spectra in the 3700–2700 cm^{-1} spectral region.

C=N stretching

The C=N stretching was found at 1670 and at 1650 cm^{-1} by deconvolution infrared band analysis, and these wavenumbers agree well with the DFT calculations.

C=O stretching and H–N–H bending

In the vibrational spectrum of the $[\text{Ni}(\text{GAA})_2]$ complex we expected to observe two $\delta(\text{HNH})$ scissoring (sciss.) and two $\nu(\text{C=O})$. Four wavenumbers can be assigned to the following vibrational modes: 1701 cm^{-1} , $\delta(\text{HNH})$ sciss., 1621 cm^{-1} , and $\delta(\text{HNH}) + \text{Q}(\text{C=O})$ indicating the coupling of the H–N–H bending and with the C=O stretching internal coordinates in the normal mode description. The 1595 cm^{-1} and 1542 cm^{-1} bands visualized by band deconvolution, assigned as $\text{Q}(\text{C=O}) + \delta(\text{HNH})$ indicating that the internal coordinates of the C=O stretching and the H–N–H bending participate in the description of the normal mode. Fig. 5 shows the band deconvoluted spectra in the 1850–1525 cm^{-1} spectral

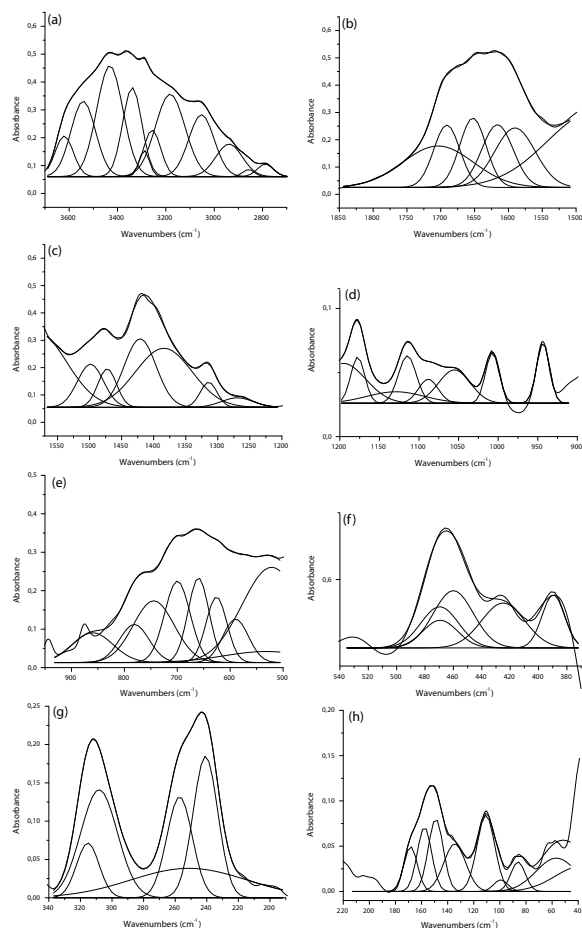


Fig. 5 Band deconvolution analysis in the (a) 3700–2700, (b) 1850–1545, (c) 1500–1200, (d) 1200–900, (e) 950–500, (f) 530–320, (g) 330–200, and (h) 220–40 cm^{-1} spectral regions.

region. Deconvolution bands were calculated using the MICROCAL ORIGIN 6 package¹⁶.

Other HNH, HCH, and rocking vibrations

In the spectral region of 1530–1420 cm^{-1} infrared bands were mainly assigned to $\delta(\text{HCH})$ sciss. and $\delta(\text{HCH})$ wagging (wagg.) vibrational modes, practically without presenting any coupling. Between 1390 and 1100 cm^{-1} the H–C–H bending was not identified as pure vibrational modes, which are constituted by coupling NH bending internal coordinates. Two $\delta(\text{HNH})$ wagg. vibrational modes can be assigned at 1171 and at 1116 cm^{-1} as being the second band confirmed in the second derivative spectrum and by deconvolution band analysis. Bands at 1113 and 1063 cm^{-1} can be assigned according to DFT calculations to: $\rho(\text{CH}_2) + \text{p}(\text{CN})$ and $\rho(\text{CH}_2) + \rho(\text{NH})$,

respectively. Rocking of the $-\text{CH}_2$ group was assigned at 941 cm^{-1} , and for the $-\text{NH}$ group at 773 and 721 cm^{-1} . In both cases not all the rocking vibrational modes could be assigned. Band deconvolution analysis of the region discussed above, that were obtained using the MICROCAL ORIGIN (Version 6.0) software¹⁶, are depicted in Fig. 5.

C–O, C–N, and C–C stretching

In the geometrical parameters of the $[\text{Ni}(\text{GAA})_2]$ structure we can determine two C–O, two C–C, and four C–N stretching internal coordinates (designated with the Latin character **p**). In the vibrational spectra of this complex we could observe only five bands which can be assigned to the following coupled modes: 1180 cm^{-1} , $\text{p}(\text{CO}) + \text{p}(\text{CC})$; 1007 cm^{-1} , $\text{p}(\text{CN}) + \delta(\text{NH})$; 910 cm^{-1} , $\text{p}(\text{CN}) + \delta(\text{NH})$ and 876 cm^{-1} , $\text{p}(\text{CC}) + \text{p}(\text{CO})$.

Framework vibrations

Assignments that involve the Ni atom coordinate in a distorted square planar geometry of C_1 symmetry are based strictly on the DFT: B3LYP/6-311G(d,p) analysis. The normal modes of this framework can be described as $\nu_{\text{as}}(\text{NiN})$, $\nu_{\text{s}}(\text{NiN})$, $\nu_{\text{as}}(\text{NiO})$, $\nu_{\text{s}}(\text{NiO})$, $\delta(\text{ONiO})$, $\delta(\text{NNiN})$, and $\delta(\text{ONiN})$. The framework of the $[\text{Ni}(\text{GAA})_2]$ complex is formed by two rings of five members, therefore no pure NiN or NiO stretching mode, as well as no pure bending mode could be found. All the normal modes of the framework structure must be defined as coupled modes formed by different internal coordinates.

For an accurate description of the normal modes in the metal-ligand spectral range, we used the percentage of deviation of the geometrical parameters (PDPG) from its equilibrium position, which constitutes the definition of the internal coordinates¹⁷. As we have pointed out earlier, the PDPG can also be normalized to obtain the percentage of participation of each internal vibrational coordinate that describes the framework vibrations.

In the description of the normal modes we used Greek letters, as usual, and in parentheses we indicate a pair of atoms for stretching or three atoms for bending, which are included in the definition of the internal coordinates. A coupled normal mode can be represented as an infinitesimal variation of single bonds or angles in time, which are the definitions of the internal coordinates that participates in the vibrational movement. A coupled normal mode is not composed of other normal modes, it is composed of several internal coordinates that describes the vibrational movement. For discussion, we have selected the spectral region

at 480–200 cm^{-1} in which we can find the metal-ligand vibrations. Naturally they are all normal modes composed of several internal coordinates and none can be considered as a pure stretching or bending. In our procedure, in which fundamental modes can be assigned, we have considered carefully the Cartesian L matrix obtained for each normal mode, used it to calculate the percentage of variation of the geometrical parameters (PDPG) values, and used these values in the description of the vibrational assignment. For the PDPG analysis, we have chosen 22 internal coordinates: 10 stretchings define the two five member rings formed by the guanidoacetic acid ligand, being represented with Latin characters: **r** for the Ni–N and Ni–O stretching, **p** for the C–C, C–O, and C–N stretching; **Q** for the C=N and C=O stretching, and there are 12 bending internal coordinates inside and outside the five member rings, all of them symbolized by β . Percentage contributions lower than 10% of the internal coordinates in the description of the normal mode are not indicated in the vibrational assignment.

The Ni–O stretching internal coordinate participates with different percentage in the vibrational modes found at: 457 cm^{-1} (calculated wavenumber), assigned as a composed mode in which mostly the internal coordinates $r(\text{NiO})$ 27% + $\beta(\text{NNiO})$ 25% participate. The infrared band observed at 373 cm^{-1} can be assigned as a vibrational mode which coupled with different internal coordinates; $\beta(\text{NNiO})$ 18% + $r(\text{NiO})$ 14% + $r(\text{NiN})$ 14% + $p(\text{NC})$ 13% + $p(\text{CC})$ 10%. Similarly, the observed band at 313 cm^{-1} can be described as the association of the following internal coordinates: $r(\text{NiN})$ 26% + $r(\text{NiO})$ 21% + $\beta(\text{NNiO})$ 16%. The deconvoluted infrared band at 240 cm^{-1} , can be described as: $r(\text{NiO})$ 27% + $\beta(\text{NNiO})$ 18% + $\beta(\text{ONiO})$ 21%. Finally, the band observed at 194 cm^{-1} can be assigned as a composition of the following internal coordinates: $\beta(\text{NNiO})$ 37% + $\beta(\text{NiNC})$ 12% + $r(\text{NiO})$ 12%.

The Ni–N stretching internal coordinate participation was found in different normal modes which can be described as: 427 cm^{-1} , $r(\text{NiN})$ 14% + $\beta(\text{NNiO})$ 10%; 436 cm^{-1} (calculated wavenumber), $r(\text{NiN})$ 29% + $\beta(\text{NNiO})$ 17% + $\beta(\text{CCO})$ 14% + $\beta(\text{NiNC})$ 12%; 377 cm^{-1} (deconvoluted band), $\beta(\text{NNiO})$ 18% + $r(\text{NiO})$ 14% + $r(\text{NiN})$ 14% + $p(\text{NC})$ 13% + $p(\text{CC})$ 10%; 313 cm^{-1} , $r(\text{NiN})$ 26% + $r(\text{NiO})$ 21% + $\beta(\text{NNiO})$ 16%; 153 cm^{-1} , $\beta(\text{NNiO})$ 47% + $\beta(\text{NiNC})$ 13% + $r(\text{NiN})$ 11%. As we can see, in the bands observed at 377 cm^{-1} and at 313 cm^{-1} the stretching character predominates.

The total assignment of the skeletal vibrational modes is presented in Table 2. Normal modes in

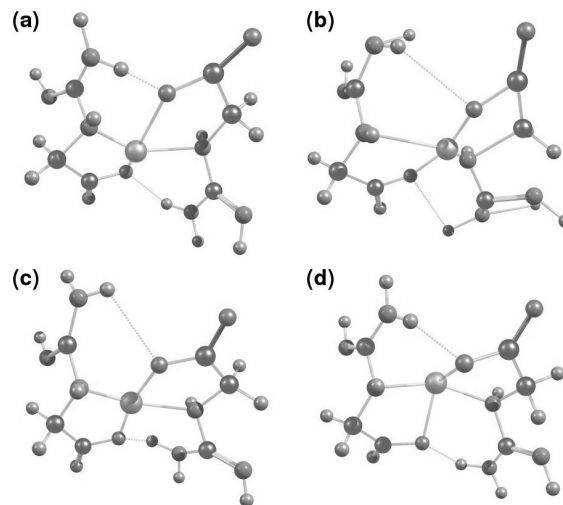


Fig. 6 Distorted geometries of some skeletal normal modes: (a) 475 (449) cm^{-1} : $r(\text{NiO})$ 27% + $\beta(\text{NNiO})$ 25%; (b) 454 (409) cm^{-1} : $r(\text{NiN})$ 29% + $\beta(\text{NNiO})$ 17% + $\beta(\text{CCO})$ 14% + $\beta(\text{NiNC})$ 12%; (c) 383 (359) cm^{-1} : $\beta(\text{NNiO})$ 26% + $\beta(\text{NiNC})$ 14% + $r(\text{NiN})$ 11%; and (d) 278 (241) cm^{-1} : $r(\text{NiO})$ 27% + $\beta(\text{NNiO})$ 18% + $\beta(\text{ONiO})$ 21%.

which mainly the Ni–O and Ni–N stretching internal coordinates participate, are depicted in Fig. 6. The figures were obtained using the CHEMCRAFT software¹⁸.

CONCLUSIONS

Synthesis, elementary CHN–O analysis, thermogravimetry and infrared spectrum of $[\text{Ni}(\text{GAA})_2] \cdot 2\text{H}_2\text{O}$ complex were presented. Theoretical calculations concerning structural analysis confirmed that the *trans*- $[\text{Ni}(\text{GAA})_2]$ complex is more stable than the *cis* conformation. Also, infrared spectrum through vibrational analysis and detailed comparison of the calculated IR-spectra in the low metal-ligand region for both isomers with the experimental spectrum, has confirmed the *trans* Ni–N and Ni–O coordination in the complex with the ligand guanidoacetic acid. Vibrational assignments of bands in the infrared spectrum of the $[\text{Ni}(\text{GAA})_2] \cdot 2\text{H}_2\text{O}$ complex have been done based on the DFT: B3LYP/6-311G(d,p) quantum mechanical calculation. For the skeletal vibrations the most probable assignment was based on the interpretation of the distorted geometry of the normal modes, having as a focus the study of the percentage of deviation of the geometrical parameters. The results suggest the structure depicted in Fig. 3 as the most probable, and the full assignment for the complex is presented in Table 2. The NBO results

indicate that the Ni–O and Ni–N bonds are formed by the interaction of the $sp^{1.8}$ (35.76% s and 64.24% p) orbital on the oxygen atom, and the $sp^{4.33}$ (18.77% s and 81.23% p) orbital on the nitrogen atom with the $sp^{2.04}d^{1.04}$ hybrid orbital of Ni.

Acknowledgements: The authors thank CNPq and CAPES for financial assistance and research grant.

REFERENCES

1. Versiane COV, Téllez SCA, Giannerini T, Felcman J (2005) Fourier-transform infrared spectrum of aspartate hydroxo-aqua nickel (II) complex and DFT-B3LYP/3-21G and 6-311G structural and vibrational calculations. *Spectrochim Acta Mol Biomol Spectros* **61**, 337–45.
2. Ramos JM, Versiane O, Felcman J, Téllez SCA (2009) FT-IR vibrational spectrum and DFT:B3LYP/6-31G and B3LYP/6-311G structure and vibrational analysis of glycinate-guanidoacetate nickel (II) complex: [Ni(Gly)(Gaa)]. *Spectrochim Acta Mol Biomol Spectros* **72**, 182–9.
3. Ramos JM, Versiane O, Felcman J, Téllez SCA (2007) FT-IR vibrational spectrum and DFT:B3LYP/6-311G structure and vibrational analysis of bis-serinenickel(II) complex: [Ni(Ser)₂]. *Spectrochim Acta Mol Biomol Spectros* **67**, 1046–54.
4. Lancaster JR (1988) *The Bioinorganic Chemistry of Nickel*, 1st edn, John Wiley & Sons.
5. Chandra S, Raizada S, Tyagi M, Gautam A (2007) Synthesis, spectroscopic, and antimicrobial studies on bivalent nickel and copper complexes of bis(thiosemicarbazone). *Bioinorg Chem Applicat*, ID 51483.
6. Banica FG, Kafar B, Skrzypek S, Ciesielski W (2006) Selenomethionine-catalyzed nickel ion reduction at a mercury electrode: Applications in the analysis of nutritional supplements. *Electroanalysis* **18**, 2269–72.
7. Ramos JM, Versiane O, Felcman J, Téllez SCA (2007) FT-IR vibrational spectrum and DFT:B3LYP/6-31G structure and vibrational analysis of guanidinoaceticserinenickel(II) complex: [Ni(GAA)(Ser)]. *Spectrochim Acta Mol Biomol Spectros* **67**, 1037–45.
8. Téllez SCA, Silva A, de M, Felcman J (2004) Fourier transform Raman spectra (in aqueous solution) of serine and tetraaqua serine aluminium (III) cation complex: [Al(Ser)(H₂O)₄]²⁺. DFT: B3LYP/3-21G structural and vibrational calculations. *J Raman Spectros* **35**, 19–27.
9. Faget OG, Giannerini T, Felcman J, Téllez SCA (2005) Fourier-transform infrared and Raman spectra of cysteine dichloride cadmium(II) anion: DFT: B3LYP/3-21G(d) structural and vibrational calculations. *Spectrochim Acta Mol Spectros* **61**, 2121–9.
10. Frisch MJ, Trucks GW, Schlegel HB, Scuseria GE, Robb MA, Cheeseman JR, Montgomery JA, Vreven T Jr et al (1998) *Gaussian 98*. Gaussian, Inc., Pittsburgh, PA.
11. Versiane Cabral O (2005) Synthesis and characterization of complexes between the amino acids serine, glycine, aspartic acid, guanidine acetic acid and metal ions Co(II), Ni(II) and Cd(II). PhD thesis, PUC-Rio.
12. Antolini L, Menabue L, Pellacani GC, Marcotrigiano G (1982) Structural, spectroscopic, and magnetic properties of diaqua(L-aspartato)nickel(II) hydrate *J Chem Soc Dalton Trans* **12**, 2541–3.
13. Addison AW (1983) Spectroscopic and redox trends from model copper complexes, in Karlin KD, Zubieta JA (eds), *Copper Coordination Chemistry: Biochemical and Inorganic Perspectives*, Adenine Press, Guilderland, NY, pp 109–28.
14. Foster JP, Weinhold F (1980) Natural hybrid orbitals. *J Am Chem Soc* **102**, 7211–8.
15. Bellamy LJ, Williams R (1957) The NH stretching frequencies of primary amines. *Spectrochim Acta* **9**, 341–5.
16. Microcal (TM) Origin Version 6.0, Microcal Software, Inc., USA. <http://www.microcal.com>
17. Ramos JM, Faget OG, Felcman J, Tellez SCA (2008) Fourier transform infrared and Raman spectra, and AB initio calculations for cadmium(II)-cysteinate glycinate complex [Cd(Cys)(Gly)]. *Spectrochim Acta Mol Biomol Spectros* **71**, 1364–70.
18. Zhurk GA, Zhurko DA (2005) ChemCraft: tool for treatment of chemical data, Lite version build 08 (free-ware).